Object Re-Orientation via Two-Edge-Contact Pushing along a Circular Path Based on Friction Estimation

Ziyan Gao, *Member, IEEE*
School of Information Science
Japan Advanced Institute of Science and Technology
Nomi, Ishikawa, Japan
ziyan-g@jaist.ac.jp

Chenghao Li, *Student Member, IEEE*
School of Information Science
Japan Advanced Institute of Science and Technology
Nomi, Ishikawa, Japan
chenghao.li@jaist.ac.jp

Dianbo Ma
School of Electrical Engineering and Computer Science
Kanazawa University
Kanazawa, Ishikawa
madb201910@stu.kanazawa-u.ac.jp

Nak Young Chong, *Senior Member, IEEE*
School of Information Science
Japan Advanced Institute of Science and Technology
Nomi, Ishikawa, Japan
nakyoung@jaist.ac.jp

***Abstract*—Achieving a stable displacement of an object to its target pose is a fundamental requirement in numerous robotic manipulation tasks. In this work, we investigate the use of planar pushing to re-orient an object with unknown physical parameters. Primarily, this study serves as a supplement to our previously introduced Zero Moment Two Edge Pushing (ZMTEP) technique designed to achieve pure object translation. Specifically, precise object re-orientation is accomplished by employing a variable stroke parallel-jaw gripper pusher to make contact with two edges of the object and execute circular motion. We initially give an assertion for enabling an unknown object to smoothly track a specified circular trajectory while remaining in sticking contact with the pusher. Subsequently, we carry out a comprehensive set of experiments to validate the suggested claim by examining the possible two-edge-contact (TEC) configurations. Lastly, we assess the practicality of the estimated frictional forces to find the achievable TEC configurations. The experimental outcomes provide empirical evidence that confirms the validity of friction estimation for TEC pushing.**

I. INTRODUCTION

Pushing is a widely recognized non-prehensile manipulation technique that can be utilized across various robotic platforms. In contrast to grasping, pushing proves to be particularly advantageous when dealing with objects that are difficult to grasp due to their shape, size, or material characteristics. Hence, pushing has been applied in a range of tasks including object rearrangement [1], target acquisition [2], singulation [3], bin picking [4], in-hand re-grasping [5], and various other tasks.

Prior studies have primarily focused on either single-contact or line-contact pushing to tackle the hybrid nature in the pusher-slider system and the constantly changing pressure distribution between the object and the sliding surface. For accurate object re-arrangement, it has been common practice to use full-state feedback of the pusher-slider system, in strict adherence to the constrained motion resulting from the restricted friction between the pusher and the object, and the modeling of object motion. However, in our earlier work [6], we introduced an innovative idea of using two-edge-contact (TEC) for precise pure object translation, along with the suggestion of zero moment two edge pushing (ZMTEP) as a method to relocate an object through open loop pushing execution. Subsequently, ZMTEP is further extended to handle objects with both unknown physical properties and imprecise shape information [7]. More precisely, by optimizing the positions of two contact points situated at distinct edges of the object, the object can be purely translated to the target position, while maintaining sticking-contact with the pusher regardless of the friction between the pusher and the object. Hence, the question arises as to whether precise object re-orientation can be accomplished through TEC pushing without feedback.

This research focuses on examining the condition of sticking contact when an object travels a circular path at a constant speed as illustrated in Fig. 1, with no intention of algorithmically determining the exact circular path. With the identified TEC configuration, the pusher can stably push the object to trace the desired circular path, irrespective of the friction between the pusher and the object. We conduct extensive experiments with a real physical robot to validate the proposed pushing manipulation. In order to deal with a novel object, we implement a frictional force estimation method proposed by Lynch [8]. We then conduct real experiments to explore the achievable TEC configurations to justify the use of the estimated frictional forces.

For the sake of simplicity, the following assumptions are made:

- The object is flat, and it does not tilt or flip during and after being pushed.
- The pusher, the object, and the support plane are rigid.
- Coulomb's law of friction applies.
- We assume quasi-static interaction between the pusher and the object, which means the system is assumed to be in equilibrium at every infinitesimal step in time, and the inertial effects are negligible compared to the dominant frictional forces.

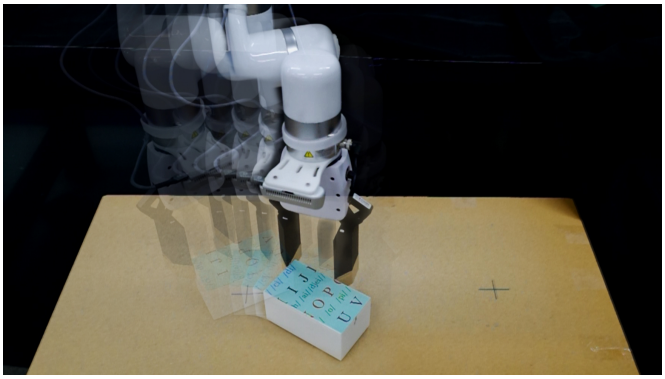

Fig. 1. A sequence of snapshots of object re-orientation using TEC pushing.

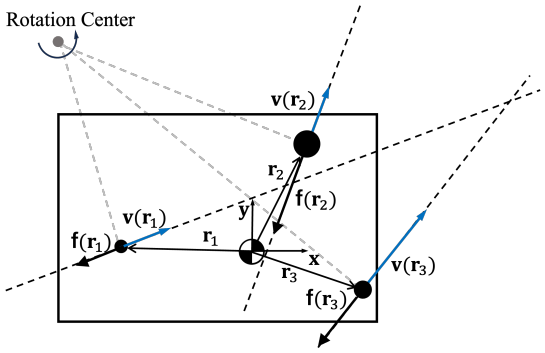

Fig. 2. Frictional forces from the sliding ground to the objects. Black dots represent the contact condition between the object and the sliding ground, and the radius of the black dot are proportional to the support forces.

II. Related Work

The previous studies [9], [10] focused on the use of open-loop pushing to reposition objects with known geometry and inertial properties using a flat pushing fence. In [11], the stable pushing by line pushing was studied, where all contacts between the pusher and the slider were collinear with contact normals perpendicular to the line. Recently, Tang *el al.* [12] re-formulated the object re-arrangement using line-contact pushing as a nonlinear model predictive control (NMPC). On the other hand, this work investigates the sticking-contact condition for achieving stable circular motion in the presence of TEC pushing. Compared to the line pushing in which the space of turning motion is constrained by the friction between the pusher and the object, we show that precise circular motion can be achieved regardless of the frictional forces between the pusher and the object if the condition stated in assertion 1 satisfies.

Under the assumption of quasi-static pushing, an ellipsoid model was derived in [13] to approximate the limit surface [14], [15] which relates the applied force with object velocity. The ellipsoid model was then used for pushing controller design as in [16], [17], [18]. However, the ellipsoid approximation needs a known CoM and friction between the pusher and the slider and it under-fits the real object motion. In this work, instead of utilizing the ellipsoid approximation, we leveraged the estimated frictional forces to estimate the required pushing force given the desired circular motion.

The object rearrangement task can also be solved by multi-step pushing. In [19], [20], end-to-end learning models were trained to predict object motion. Then, a series of pushing actions were planned to achieve the goal pose. The authors in [21] showed the exact step bound for a given object rearrangement task and a set of known line pushes with known pushing effects. However, these methods lack efficiency, as the number of pushes is proportional to the difference between the initial and target object poses. In this study, we demonstrate that object re-orientation can be effectively achieved through achievable TEC pushing.

III. METHOD

The objective of this study is to identify possible configurations with two edge contacts that enable constant circular motion without causing sliding between the pusher and the object. As the object moves on the surface, the frictional force, in accordance with Coulomb's law of friction, is independent of the sliding speed and acts opposite to the direction of motion.

A. The line of resultant of frictional forces

To analyze the resultant of frictional forces, a local coordinate frame is attached to the center of mass (CoM) of the object. Let $\mathbf{r_i}$ denote the i-th ground contact point and $\mathbf{v}(\mathbf{r_i})$ its velocity. Let also μ_g denote the Coulomb friction coefficient. The frictional forces at $\mathbf{r_i}$ is represented by $-\mu_g \frac{\mathbf{v}(\mathbf{r})_i}{\|\mathbf{v}(\mathbf{r_i})\|}$. Fig. 2 illustrates three frictional forces while the object rotates around the given rotation center.

The resultant (combined effect) of frictional forces is represented by $(\mathbf{F}_f, M_f)$, where $\mathbf{F}_f$ refers to the sum of frictional forces at all contact points between the object and the ground, while M_f refers to the total frictional moment exerted by the ground about the z-axis of the local coordinate frame, respectively, given by Eq. 1 and Eq. 2.

$$\mathbf{F}_f = \Sigma_i \mathbf{f}(\mathbf{r_i}) \tag{1}$$

$$M_f = \Sigma_i \mathbf{r_i} \times \mathbf{f}(\mathbf{r_i}) \tag{2}$$

In this work, the resultant of the frictional forces acting on the object from the sliding ground is referred to as the ground resultant.

When an object undergoes pure translation which is a rotation with the center of rotation at infinity, the line of ground resultant passes through the object CoM. In the general case, the line of ground resultant is parameterized by the $(\mathbf{F}_f, M_f)$. The slope of the line of resultant is specified by the direction of $\mathbf{F}_f$, and the distance between the line of ground resultant and the frame located at the object CoM is $\frac{M_f}{\|\mathbf{F}_f\|}$.

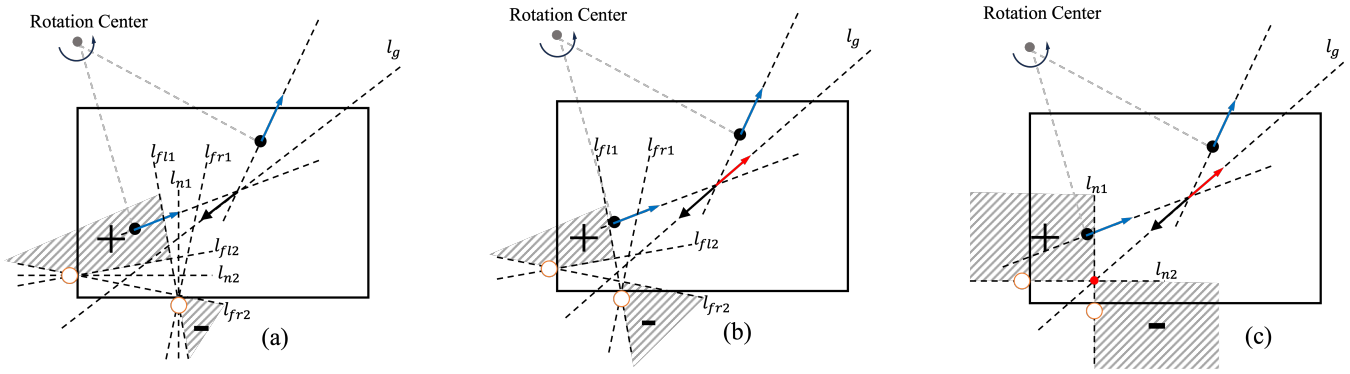

Fig. 3. Illustration of moment labels for TEC configurations and the ground resultant when the object undergoes circular motion. The hatched region are the moment labels. The ground resultants are shown in black arrows and the lines of the ground resultants are represented by black dotted lines.

B. Two Edge Contact Configuration

Consistent with our previous research [6], the TEC configuration is characterized as $(\mathbf{cp}_1, \mathbf{cp}_2, \mathbf{n}_1, \mathbf{n}_2)$, with $\mathbf{cp}_*$ representing the contact point between the pusher and the object, and $\mathbf{n}_*$ indicating the normal direction at the pusher-object contact point. Subsequently, multiple lines, l_{n*}, l_{fl*}, l_{fr*}, are defined following the methodology outlined in [6], where l_{n*}, l_{fl*}, l_{fr*} indicate lines that intersect the contact position $*$ and align with the contact normal direction, as well as the left and right boundaries of the friction cone. In addition, we define l_g that represents the line of ground resultant.

C. Quasi-Static Analysis

Under quasi-static conditions, to balance the ground resultant, the pusher must exert a contact force to the object opposite to the ground resultant. In this work, we aim to generate such a pushing force using two-edge-contact (TEC) pushing. Given a TEC configuration, the planar wrench cone of two pushing forces can be represented using moment labels. Fig. 3 illustrates moment labels for three TEC configurations. The pusher can only generate the contact forces which have consistent sign of moment to the labeled hatch region as shown in Fig. 3.

In Fig. 3, assume for simplicity that there are only two frictional forces acting between the object and the ground. The ground resultant can be calculated by referring to the rotation center and the direction of rotation, as depicted by the black arrow in Fig. 3. To fulfill the sticking contact condition with the object, the line of the ground resultant depicted by the black dashed line should not intersect with the hatched area, as depicted in an unacceptable scenario in Fig. 3(a). If the line of the feasible pushing force aligns with the line of the ground resultant, the object can smoothly follow the intended circular path without breaching the sticking contact condition. An illustration of this scenario is depicted in Fig. 3(b).

The special case arises when the frictional coefficient between the pusher and the object is equal to zero. In this case, all pushing forces must pass through the intersection point denoted by $l_{n1} \cap l_{n2}$. Therefore, to meet the sticking contact requirement, the line of ground resultant must pass through $l_{n1} \cap l_{n2}$. In other words, the sticking contact requirement can be satisfied only if l_{n1}, l_{n2}, l_g intersect at a single point, and two contact normals can positively span the required pushing force.

Assertion 1: Given a fixed rotation center with corresponding ground resultant, if there exists a TEC configuration with which the corresponding contact normal forces positively span the required pushing force for balancing the ground resultant, also l_{n1}, l_{n2} and l_g intersect at a single point, then the object can follow the pre-specified circular path using this TEC configuration without breaking the sticking contact requirement.

The assertion 1 claims a sufficient condition for achieving sticking contact circular pushing. Since forces aligned with the contact normal direction can always be produced at each contact point between the pusher and the object, regardless of the presence of tangential force between the pusher and the object.

IV. Experiment

In this work, we conducted two experiments. The first experiment aims to verify the assertion 1. The second experiment involves the verification of the utility of the estimated ground resultant for TEC selection. Specifically, the second experiment includes estimating the frictional forces between the object and the ground as it slides, investigating various possible TEC configurations under different turning radius and frictional conditions.

A. Experimental Setup

The configuration for the experiment is shown in Fig. 4, where an RGB-D vision sensor is mounted at the end link of the robotic arm, capturing the top view of the object. We 3D printed a grid box and four feet that can be mounted at the bottom of the grid. Lead blocks are inserted into the grid box to vary the CoM of the grid box, while the positions of the

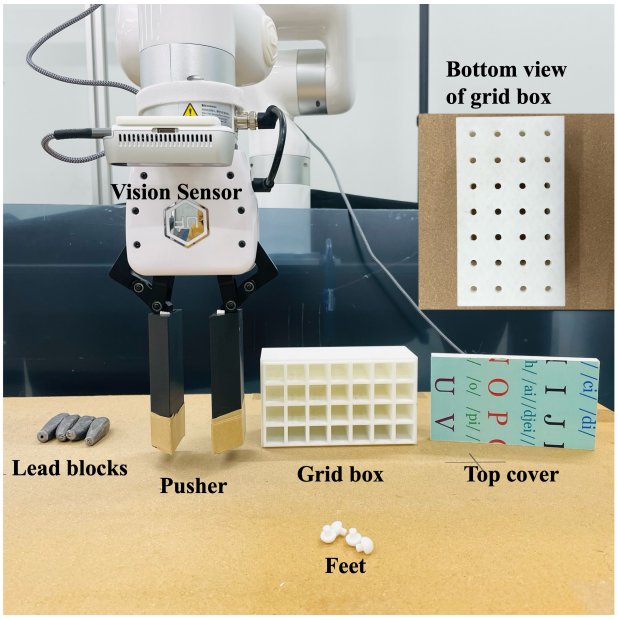

Fig. 4. Experimental setup with the pusher wrapped by Kraft paper.

feet are adjusted to vary the contact points between the grid box and the sliding ground.

A textured surface paper is adhered to the top cover of the object to track the variations in the position of the pushed object using the Scale Invariant Feature Transform (SIFT) [22]. Before starting the pushing motion, the robotic arm modifies its joint angles to guarantee that the entire shape of the object is visible within the view of the camera. The camera records the pushing action at a frequency of $16.7Hz$. Key points and their descriptors are extracted from each captured image frame. The projective transformation matrix is then calculated by matching the keypoints between the registered image and each image frame using a brute force matcher and Lowe's test ratio. The difference in object pose from the pose before the object is pushed can be acquired by decomposing the projective transformation matrix.

The experimental setup includes both high-frictional and low-frictional pushing. In low friction pushing, we use the pusher with a Kraft wrap, while in high friction pushing, the pusher is wrapped by rubber. In the high friction setting, the frictional coefficient between the pusher and the objects is found to be 0.70. In the low friction setting, the frictional coefficient between the pusher and the objects is 0.38.

B. Validation on the assertion

In this experiment, the robot is commanded to make TEC to perform a circular motion *w.r.t.* a stationary rotation center. Specifically, the feet are mounted at corners of the grid box, and the lead block configuration are shown in Fig. 6. In this scenario, the object's CoM overlaps the geometric center (*a.k.a.* the centroid) of the grid box, and the frictional force at each foot is of the same magnitude. We calculate the ground resultant manually for verification, using the specified rotation center.

The objective is to rotate the object by sixty degrees following the circular path. The TEC arrangement is regarded as achievable if the ultimate orientation deviation is under 5 degrees and the amount of sliding between the pusher and the object is less than 5 millimeters. To find the achievable TEC configurations for this task, we uniformly select several contact points from two edges of the object. Due to hardware constraints (the stroke length limits of the parallel-jaw gripper), only contact points from adjacent edges are combined. We automate the process of finding achievable TEC configurations, using ZMTEP with annotated object CoM to translate the object to the initial position if the generated pusher path is beyond the robot kinematic limit. The pipeline is shown in Fig. 5.

The outcome of this experiment is depicted in Fig. 6. To better show the result, each sub-figure in Fig. 6 displays TEC configurations sampled from same two edges of the grid box, and each TEC configuration is visualized by using the intersection point of $l_{n1} \cap l_{n2}$ specified by that TEC configuration. The intersection points are highlighted as red crosses and orange dots. The red cross infers failure of the task, while the orange dot infers the success of the task. The force for balancing the ground resultant is illustrated by a prominent yellow arrow in Fig. 6. Please note that the line of ground resultant l_g is coincident with the yellow prominent arrow.

Based on Fig. 6, with the exception of the configurations in the third sub-figure, all of the TEC configurations depicted in Fig. 6 are unsuccessful in accomplishing the task. This phenomena aligns with the assertion 1 which states that two contact normal directions should positively span the required pushing force. Furthermore, intersection points $l_{n1} \cap l_{n2}$ of achievable TEC configurations exhibit a symmetrical distribution along the prominent yellow arrow. The proximity of the intersection point to the yellow arrow corresponds to a decrease in the magnitude of the error. This observation supports the assertion 1 that l_{n1}, l_{n2} and l_g coincident with the prominent yellow arrow should intersect at a single point. Moreover, the quantity of intersection points rises in the direction of the arrowhead, mirroring the concept of contact tolerance analysis discussed in [6].

C. Validation on the estimated ground resultant for TEC selection

The outcome of the initial experiment demonstrates that identifying the line of ground resultant l_g enables the determination of attainable TEC configurations through the investigation of the presence of the intersection point $l_{n1} \cap l_{n2}$ on l_g. Therefore, for precisely re-orienting novel object, the frictional forces between the object and the ground should be estimated in order to calculate the line of ground resultant l_g.

To estimate the frictional forces, we implement the method proposed in [8] which utilized a linear programming formulation to estimate the normalized magnitude of the friction forces between the object and the ground. We discovered that

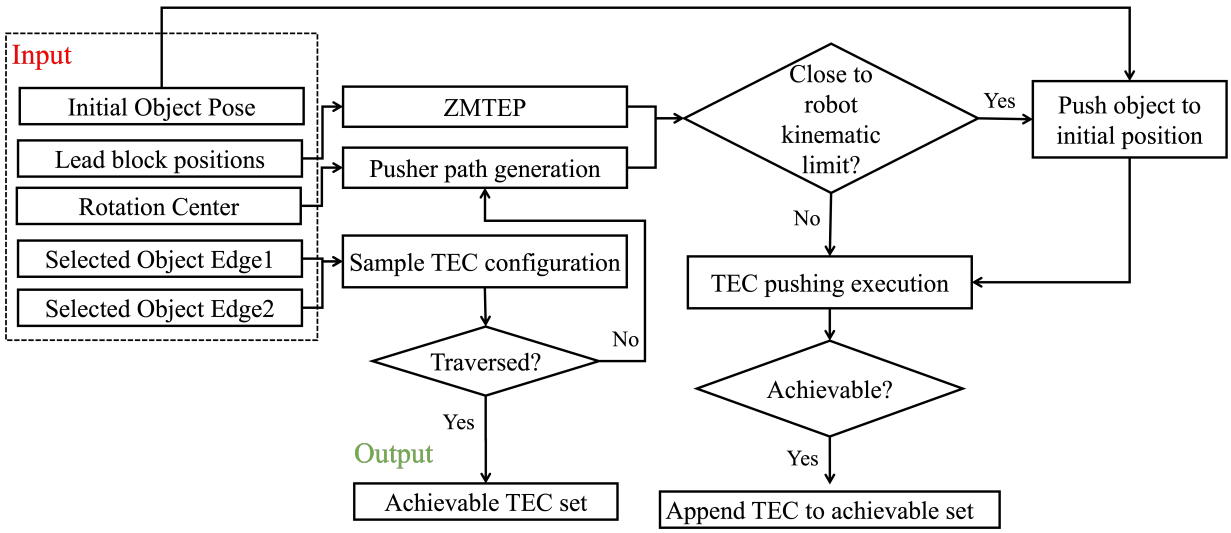

Fig. 5. Pipeline for finding achievable TEC configurations.

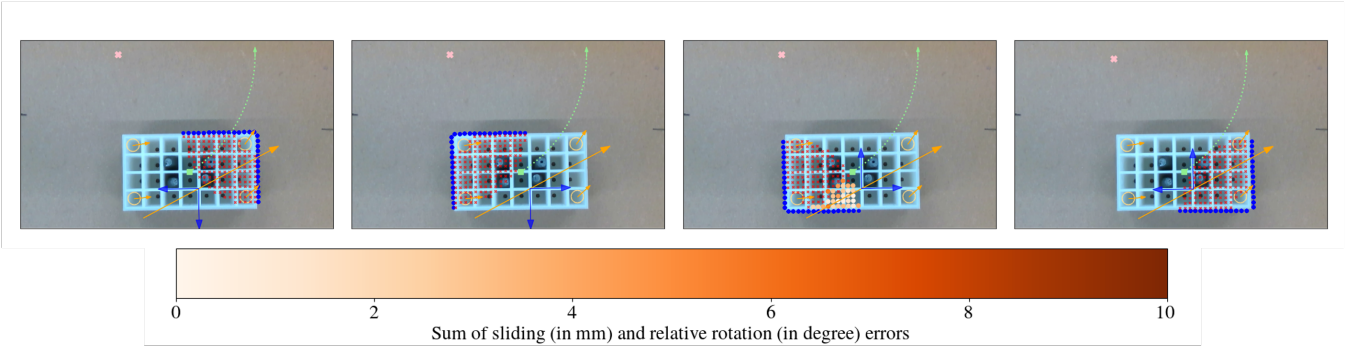

Fig. 6. Visualization of the outcome of the first experiment. Each subplot displays the outcome of TEC setups obtained from identical pairs of edges. The sampled contact points are shown in blue dots. The stationary rotation center is shown by pink cross. We use light green square marker to illustrate the object center of mass, and light green dashed line to show the desired trajectory of the object. Yellow circles depict the mounted feet and small yellow arrows the directions of velocities at feet. The desired contact force for balancing the resultant of the frictional forces are drawn by prominent yellow arrow. Blue arrows represent normal directions of two contact points. The color of the orange dot represents the summed error. The larger the error is, the darker the dot.

a quadratic objective function yields more accurate results, and reformulated the problem as a quadratic programming problem. Specifically, a number of contacts points between the novel object and the ground are hypothesized, each of which has a corresponding non-negative weight representing the normalized magnitude of the frictional forces. The goal is to optimize the weights by minimizing the magnitude of the moment at the contact point between the pusher and the object under the assumption of quasi-static interaction.

This experiment is conducted as follows. Firstly, we conduct three estimation experiments. In each estimation experiment, the lead block configurations are kept the same while the positions of the feet are different as shown by the orange circles in Fig. 7. In each estimation experiment, eight single-contact pushing interactions are conducted to collect the synchronized pusher-object motion. The contact points between the pusher and the object are uniformly selected as in [8]. For each pushing interaction, the robot pushes the object $5cm$ along the estimated contact normal direction at each contact point. After collecting the synchronized pusher-object motion, we use quadratic programming to estimate the weight of each hypothesized contact point between the object and the ground.

Secondly, we apply the same procedure as shown in Fig. 5 to find the achievable TEC configurations to verify the use of estimated frictional forces for calculating l_g. Different from the first experiment, two circular motions with different turning radius are considered for estimated ground resultant verification. In addition, to study the effect of the friction between the pusher and the object on the achievable set of TEC configurations, both high- and low- frictional pusher are leveraged. To efficiently explore the achievable set of TEC configurations, given the estimated ground resultant, the TEC configurations are sampled solely from edges whose corresponding contact normals can positively span the required pushing force based on the assertion 1. We apply the same metric as the one in the first experiment to determine if it is

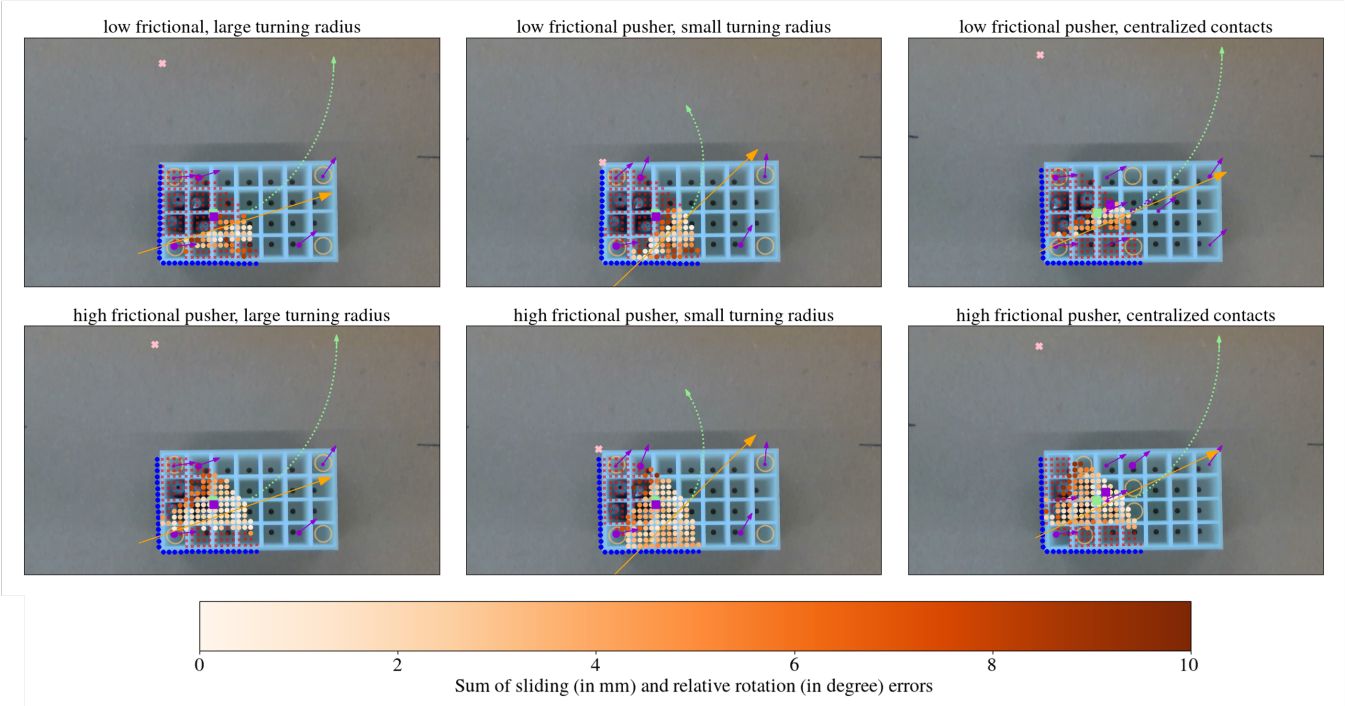

Fig. 7. Illustration of the result of the second experiment. The positions of the feet in the first two columns of the figure are the same, while the sub-figures in the last column are different. The estimated support forces are illustrated using purple dots, and the size of the dot is proportional to the estimated frictional force at that position. The estimated object CoM is illustrated by purple square. Given the stationary rotation center, the directions of the velocities at the estimated contact points between the object and the sliding ground are drawn using purple arrows. The sub-figures in the first and the last columns show results of circular motion with larger turning radius while sub-figures in the middle shows results of circular motion with smaller turning radius.

achievable or not.

The estimation results and the achievable set of TEC configurations are shown in Fig. 7. Consistent with Fig. 6, we use prominent yellow arrow, which also depicts the line of ground resultant, showing the estimated required pushing force. The purple dots represent the estimated frictional forces, with the dot size indicating the force magnitude. The findings indicate that the estimated pushing force, as shown by the prominent yellow arrow, provides compelling evidence for selecting the TEC configuration, even though there are discrepancies between the estimated frictional forces and the real contact conditions, which introduce some bias in the estimated yellow arrow compared to the observations in the initial experiment.

Comparing the first and second columns of Fig. 7, circular motions of large and small turning radius are executed. We observed that the line of ground resultant depicted by yellow prominent arrow changes while the achievable set of TEC configurations varies accordingly. However, as evidenced in the figure, the lines of the estimated required pushing force are not evenly split the intersect points of the set of achievable TEC configurations, because of the estimation error in frictional forces.

The effect of the friction between the pusher and object to the set of achievable TEC configurations can be seen by comparing the first and the second row of Fig. 7. The top row of Fig. 7 displays outcomes obtained with a low-friction pusher, whereas the bottom row presents results achieved with a high-friction pusher. In comparison to these two rows, the number of possible TEC arrangements is greater when a high-friction pusher is employed. The increase in quantity is a result of the enhanced contact tolerance as the friction between the pusher and the object is increased [6].

When comparing the results of the first and the last columns of Fig. 7, where separated and centralized feet are mounted on the grid box. Even though object CoMs are the same, the change in positions of feet affects the distributions of the achievable pushing set, while the estimated required pushing force changed correspondingly.

V. CONCLUSIONS

In this work, we propose to achieve object re-orientation using TEC pushing. It states that if the the contact normals can positively span the direction of required pushing forces, and lines of contact normals and the line of ground resultant intersect at a single point, the object can achieve the desired circular motion by using the TEC configuration. We conducted extensive real experiments to verify the proposed method. We also conducted experiments to verify the utility of using the estimated frictional forces to find the achievable TEC configuration. The result showed that the estimated frictional forces provide strong evidence for finding the achievable TEC configurations for object re-orientation.

There are several potential works required to be addressed in the future. Firstly, comprehensive comparison between

single-contact, line-contact and the two-edge contact will be performed to further validate the benefits of the proposed method. Secondly, we observed variations in the frictional forces over time. Studying on efficiently and accurately estimating frictional forces would be an interesting research direction. In addition, we assumed in this work the direction of contact normals are known. Re-orienting the novel object with unknown contact normals would be a potential future work. Lastly, the rotation centers were specified manually, based on the estimated frictional forces. Finding the instantaneous center of rotation to achieve the minimum turning radius can help re-arrange the object in confined space which can lead a broad potential application of the use of planar pushing for object re-arrangement.

ACKNOWLEDGMENT

This work was supported by JSPS KAKENHI Grant Number JP23K03756.

REFERENCES

[1] C. Song and A. Boularias, "Object rearrangement with nested nonprehensile manipulation actions," in *2019 IEEE/RSJ International Conference on Intelligent Robots and Systems (IROS)*, 2019, pp. 6578–6585.

[2] B. Huang, S. D. Han, A. Boularias, and J. Yu, "Dipn: Deep interaction prediction network with application to clutter removal," in *2021 IEEE International Conference on Robotics and Automation (ICRA)*. IEEE, 2021, pp. 4694–4701.

[3] A. Eitel, N. Hauff, and W. Burgard, "Learning to singulate objects using a push proposal network," in *Robotics Research: The 18th International Symposium ISRR*. Springer, 2020, pp. 405–419.

[4] M. Danielczuk, J. Mahler, C. Correa, and K. Goldberg, "Linear push policies to increase grasp access for robot bin picking," in *IEEE International Conference on Automation Science and Engineering*, 2018, pp. 1249–1256.

[5] N. Chavan-Dafle, R. Holladay, and A. Rodriguez, "Planar in-hand manipulation via motion cones," *The International Journal of Robotics Research*, vol. 39, no. 2-3, pp. 163–182, 2020. [Online]. Available: https://doi.org/10.1177/0278364919880257

[6] Z. Gao, A. Elibol, and N. Y. Chong, "Zero moment two edge pushing of novel objects with center of mass estimation," *IEEE Transactions on Automation Science and Engineering*, vol. 20, no. 3, pp. 1487–1499, 2023.

[7] ——, "On the generality and application of mason's voting theorem to center of mass estimation for pure translational motion," *IEEE Transactions on Robotics*, vol. 40, pp. 2656–2671, 2024.

[8] K. M. Lynch, "Estimating the friction parameters of pushed objects," in *IEEE/RSJ International Conference on Intelligent Robots and Systems*, 1993, pp. 186–193.

[9] S. Akella and M. T. Mason, "Posing polygonal objects in the plane by pushing," *The International Journal of Robotics Research*, vol. 17, no. 1, pp. 70–88, 1998. [Online]. Available: https://doi.org/10.1177/027836499801700107

[10] Q. Li and S. Payandeh, "Manipulation of convex objects via two-agent point-contact push," *The International Journal of Robotics Research*, vol. 26, no. 4, pp. 377–403, 2007. [Online]. Available: https://doi.org/10.1177/0278364907076819

[11] K. M. Lynch and M. T. Mason, "Stable pushing: Mechanics, controllability, and planning," *International Journal of Robotics Research*, vol. 15, no. 6, pp. 533–556, 1996. [Online]. Available: https://doi.org/10.1177/027836499601500602

[12] Y. Tang, H. Zhu, S. Potters, M. Wisse, and W. Pan, "Unwieldy object delivery with nonholonomic mobile base: A stable pushing approach," *IEEE Robotics and Automation Letters*, vol. 8, no. 11, pp. 7727–7734, 2023.

[13] K. Lynch, H. Maekawa, and K. Tanie, "Manipulation and active sensing by pushing using tactile feedback," in *IEEE/RSJ International Conference on Intelligent Robots and Systems*, 1992, pp. 416–421.

[14] S. Goyal, A. Ruina, and J. Papadopoulos, "Planar sliding with dry friction part 1. limit surface and moment function," *Wear*, vol. 143, no. 2, pp. 307–330, 1991. [Online]. Available: https://www.sciencedirect.com/science/article/pii/0043164891901043

[15] ——, "Planar sliding with dry friction part 2. dynamics of motion," *Wear*, vol. 143, no. 2, pp. 331–352, 1991. [Online]. Available: https://www.sciencedirect.com/science/article/pii/0043164891901054

[16] F. Bertoncelli, F. Ruggiero, and L. Sabattini, "Linear time-varying mpc for nonprehensile object manipulation with a nonholonomic mobile robot," in *2020 IEEE International Conference on Robotics and Automation (ICRA)*, 2020, pp. 11 032–11 038.

[17] J. Zhou, Y. Hou, and M. T. Mason, "Pushing revisited: Differential flatness, trajectory planning, and stabilization," *International Journal of Robotics Research*, vol. 38, no. 12-13, pp. 1477–1489, 2019. [Online]. Available: https://doi.org/10.1177/0278364919872532

[18] F. R. Hogan, E. R. Grau, and A. Rodriguez, "Reactive planar manipulation with convex hybrid mpc," in *2018 IEEE International Conference on Robotics and Automation (ICRA)*, 2018, pp. 247–253.

[19] J. K. Li, W. S. Lee, and D. Hsu, "Push-net: Deep planar pushing for objects with unknown physical properties," in *Robotics: Science and Systems*, 2018.

[20] Z. Gao, A. Elibol, and N. Y. Chong, "A few-shot learning framework for planar pushing of unknown objects," *Intelligent Service Robotics*, vol. 15, no. 3, pp. 335–350, 2022.

[21] C.-Y. Chai, W.-H. Peng, and S.-L. Tsao, "Object rearrangement through planar pushing: A theoretical analysis and validation," *IEEE Transactions on Robotics*, vol. 38, no. 5, pp. 2703–2719, 2022.

[22] D. G. Lowe, "Object recognition from local scale-invariant features," in *Proceedings of the seventh IEEE international conference on computer vision*, vol. 2. Ieee, 1999, pp. 1150–1157.